Measurement of Impedance-Frequency Property of Traction Network using Cascaded H-bridge Converters: Device Design and On-site Test

Mingli Wu, *Member, IEEE*, Jing Li, *Student Member, IEEE*, Qiujiang Liu, Shaobing Yang, *Member, IEEE*, and Marta Molinas, *Member, IEEE*

***Abstract*—To investigate the harmonic resonance in electric railways, determination of the traction network impedance using a utility instrument is an important and challenging task. This paper presents a novel industrial test device which can directly measure the impedance of the actual traction network which is the power source of the railway. The structure arrangement and the parameter design are accomplished to meet the requirements for high-voltage level and strong anti-electromagnetic interference capability. Following this, frequency-dependent impedance measurement is implemented through the injection of controlled harmonic currents using the cascaded H-bridge converters. Furthermore, the power flow analysis is carried out to demonstrate that this device does not need any additional power source and can generate harmonic power. In a new-built railway, this device has been adopted to conduct the on-site test of the traction network impedance. Then, the multi-conductor simulation model is established for the purpose of mutual verification between the field test result and simulation result. Furthermore, the on-site test results can be applied to determine the resonance frequency before a nenw-built line is put into use so that any harmonic resonance can be avoided by taking effective measures in advance.**

***Index Terms*-- Frequency-dependent, impedance, industrial device, traction network, on-site test.**

I. Introduction

THE traction network provides the single-phase electric power for the trains (also called as locomotives) whose traction drive systems are the power electronics dominated systems. Due to the influence of the harmonic current of the power electronic converters on the impedance network of the locomotive-network system, the harmonic resonance accidents of different frequencies have occurred in some railway lines [1, 2]. The accuracy of the impedance of the traction network is important for investigating the harmonic resonance accidents in the electric railway [3]. In addition, the performance of the mitigation measures would be evaluated by the impedance-frequency characteristics of the traction network [4-6]. Therefore, there is a need for acquiring the impedance of different harmonic frequencies.

It is desirable to be able to directly measure the frequency-dependent impedance of the actual traction network using a practical device. Many calculations and simulations have been performed on impedance-frequency characteristics of the traction network. In [7, 8], the traction network impedance at the location of the locomotive is calculated by applying the theory of wave propagation into the equivalent lumped parameter circuit of the contact line. In [9], a nodal admittance matrix is derived by reviewing the entire network as a composite chain circuit which is made up of serial elements and shunt elements. In [10], the eight-port transmission line model of the Korean double-track railway is established in PSCAD/EMTDC by regarding some conductors as one conductor electrically. However, the impedance representation of the traction network characterizes the frequency response of the entire traction power supply system. Both the calculation and the simulation of the impedance of traction network need detailed information of the utility grid, the substation transformer, and the distributed parameters of the contact feeder section [11-13]. Furthermore, the impedance of the utility grid which is the three-phase power source for the electric railway also affects the impedance of traction network while it is ignored in the equivalent impedance of the substation [14]. And it is impossible to accurately calculate the grid impedance at harmonic frequency by the fundamental impedance. To overcome these disadvantages, a practical device should be developed to measure the impedance of the actual traction network in electric railway systems.

Several methods have been developed to measure the frequency-dependent impedance. In the previous literature, impedance is measured through the temporary transient signals created by switching the capacitor banks, thyristor-controlled short circuit, and so on [15, 16]. The main problem associated with the transient-based method is that the impedance accuracy relies on the high performance of analog/digital (AD) conversion and the noise-elimination technique, because the transient signal usually dies out within one cycle [17, 18]. Then, in [19], a power electronic converter is employed to inject a voltage transient with 160ms duration, which can be triggered at any time. In addition, grid impedance of a broad frequency range is measured through

This work was supported in part by the Fundamental Research Funds for the Central Universities (2018JBZ101) (Corresponding author: Mingli Wu and Qiujiang Liu)

Mingli Wu, Jing Li, Qiujiang Liu, Shaobing Yang are with the School of Electrical Engineering, Beijing Jiaotong University, Beijing, 100044, China. (e-mail: mlwu@bjtu.edu.cn, 16117381@bjtu.edu.cn, qjliu@bjtu.edu.cn, shbyang@bjtu.edu.cn).

Marta Molinas is with the Department of Engineering Cybernetics, Norwegian University of Science and Technology, Trondheim 7491, Norway (e-mail: marta.molinas@ntnu.no).

injecting the maximum-length binary sequence (MLBS), or discrete-interval binary sequence (DIBS) into the current controller of the grid-connected inverter [20]. For these approaches, however, it is not easy to guarantee the spectra excitation in a frequency range of interest. Instead of a voltage/current disturbance, the controllable harmonics can be directly injected by photovoltaic (PV) inverter [21]. The impedance at different frequencies is obtained by frequency sweeping. To conclude, the controlled harmonic injection provides a good solution for the measurement of the traction network impedance as it is convenient to obtain the impedance of a certain frequency.

Some measurement units based on controllable harmonics injection have been developed. However, when the devices are applied in actual measurement, the practical constraints should be taken into consideration. A variety of inverter-based equipment injects harmonics to conduct grid impedance test in laboratories [22]. The need for the extra DC source is a non-trivia problem for actual measurement in an electric railway. In addition, the signal generator connected with an amplifier is a solution to inject harmonics into the network while the traction power should be switched off [23]. A modular silicon carbide (SiC) converter is used to measure the small-signal *dq*-domain impedance (frequency range, 5Hz~1kHz) of the three-phase AC and DC interfaces based on the single-phase injection of the series and shunt perturbation [24]. In addition, the transformerless series injector is implemented through the paralleled H-bridge converters in order to measure the small-signal impedance of the power electronics load [25]. The 11-level cascaded H-bridge inverter topology which is supplied by the mutli-winding transformer is developed to fulfill the small-signal impedance measurement of both the three-phase source and the load through different topology of the same cells [26]. But every cell of this topology comprises an input LC filter, an active front-end rectifier, and an H-bridge inverter, so that the controller overburdens due to the huge system and complex control strategy. Then, in the electric railway, the active power filter (APF) is designed to improve the power quality by compensating the harmonics and reactive power [27]. However, the APF cannot be used as a regular harmonic source because the injection frequency is only up to 1000Hz.

Accordingly, this paper focuses on designing a measurement device for on-line impedance measurement of the traction network which is the electric power source of the electric railway. The AC/DC converter, consisting of cascaded single-phase H-bridges, injects harmonic currents with controllable amplitudes and frequencies into the traction network. Firstly, without inverters, the device draws power only from the traction network directly so there is no need for an extra power source. Secondly, the device can generate harmonics of a wide range frequency which can cover the frequency range of the harmonic resonance. Thirdly, the cascaded structure of the H-bridge with phase-shifted carrier PWM gives a less distorted voltage waveform which can decrease the influence of the noise pollution of high frequencies. Moreover, it is not necessary to switch off the traction power during the on-site test so that the influence of utility grid on the impedance characteristic is taken into account.

The rest of this paper is organized in the following manner: In Section II, the structure design and main circuit parameters of the device are described. Section III introduces the implementation method of this device. Following this, in Section IV, the field test is conducted in a new line and the impedance analysis result is displayed. Finally, in Section IV, some conclusions are drawn.

II. Implementation Of The Device

A. Structure design and parameters determination

For a device which can be used in an actual railway, the structure and parameters should be researched in order to meet the requirements of on-site measurement. All of the components are designed in a cabinet so that it can be easily moved during the on-site test.

(a) The arrangement diagram of the hardware

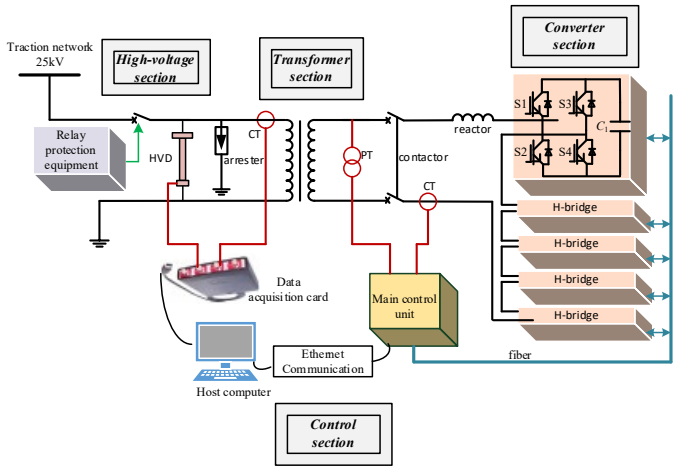

(b) The function and the components of all the sections

Fig. 1. The architecture of the device for the on-site test

The architecture of this device is displayed in Fig. 1. The overall arrangement diagram of the hardware and the components of all the sections are presented in Fig. 1(a) and (b) respectively. As shown in Fig. 1(a), the device is composed of four parts which are integrated into one cabinet for ease of

transport: high-voltage section, transformer section, converter section, and control section. The transformer section is placed in the middle of the cabinet. The converter section and the control section are located on the left side. The high-voltage section is on the right side.

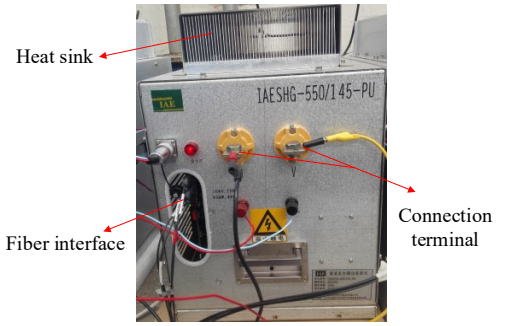

(a) The overall appearance of the module

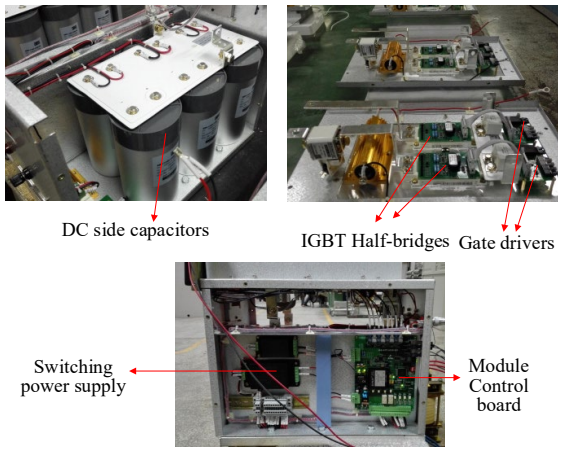

(b) The main components of the module

Fig. 2. The single-phase H-bridge (SHB) module

The function and the components of these four sections are illustrated in Fig. 1(b). Firstly, the *high-voltage section* includes the high-voltage circuit breaker which connects the traction network of the electric railway and the main circuit of the test device. When the test device is installed in the traction network, safety and stability are the most important factors for the normal operation of the electric railway. Therefore, a relay protection system is designed to open the circuit breaker when the abnormal situation of the device occurs in order to avoid serious influence on the traction network. The data acquisition card samples the voltage signal by a high-voltage divider (HVD) and the current signal by a current transformer (CT). Secondly, in the *transformer section*, a step-down transformer is an effective solution to reduce the voltage level of the cascaded single-phase H-bridge (CSH). Thirdly, the *converter section* consists of six single-phase H-bridge modules in series. One module is auxiliary in case that some module fails. Finally, *the control section* which is the core part of this device comprises two key parts. One is the main control unit where the layer control algorithm is implemented through the digitally discretization process. The CSH can inject the harmonic current into the traction network through the control algorithm. The other one is the host computer which can calculate the impedance of the traction network and monitor the running state of the entire system.

CSH modules play an important role in injecting the harmonic current into the traction network which is a 25kV single-phase system. To fulfill the requirements of realistic practice and cost effectiveness, the voltage level and the number of CSH module are decreased by utilizing a step-down transformer. In order to decrease the leakage inductance of the transformer, the shell type transformer with the structure of the wound core is adopted.

TABLE I
The Numbers of Devices' Elements for *l*-level Voltage

	DNPC	FCNPC	SHB	FBMMC
Switching element	2(*l*-1)	2(*l*-1)	2(*l*-1)	2(*l*-1)
Antiparallel diode	2(*l*-1)	2(*l*-1)	2(*l*-1)	2(*l*-1)
Clamping diode	(*l*-1)(*l*-2)	0	0	0
Clamping capacitor	0	(*l*-1)(*l*-2)/2	0	0
DC bus capacitor	(*l*-1)	(*l*-1)	(*l*-1)/2	(*l*-1)
Total number	l^2+2*l*-3	(l^2+7*l*-8)/2	9(*l*-1)/2	5(*l*-1)

With the development of power electronics, converters with different topologies are widely used in the high-voltage high-power fields. Considering that the traction network is a single-phase system, only the single-phase converters can be cascaded to inject the harmonic current into the traction network, such as the single-phase diode neutral-point-clamped three-level converter (DNPC), the single-phase fly-capacitor neutral-point-clamped three level converter (FCNPC), the single-phase full bridge modular multilevel converter (FBMMC), and the single-phase H-bridge (SHB). Table I displays the numbers of devices for the same level *l*. Taking both the numbers of devices and the complexity of control strategies into consideration, we adopt SHB as the basic unit of the device's power electronic circuit.

Each SHB module of the CSH includes two 1200V/300A IGBT (Insulated Gate Bipolar Transistor) half-bridges. The module is illustrated in Fig. 2(a). The five modules are in series through the connection terminals. The fibers are used for the communication with the main control unit and the host computer. In addition, as shown in Fig. 2(b), the DC side capacitors, the gate drivers, and the switching power supply are assembled in the module. The module control board provides protection for the SHB module, such as the overvoltage protection, the overcurrent protection, and the overheating protection so on.

It is of great importance to set proper parameters for the

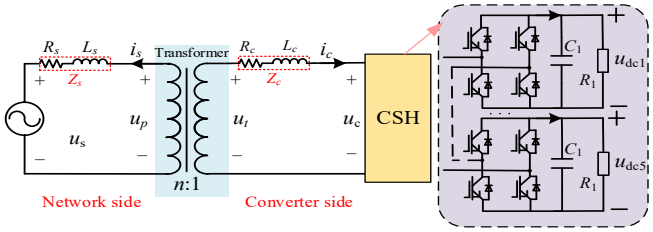

Fig. 3 The simple equivalent circuit of the test device connected to the traction network

test device due to its application in field tests. For better accuracy of the impedance test, it is necessary to inject a high harmonic current into the traction network. The simple equivalent circuit is shown in Fig. 3. The circuit equations can be expressed as:

$$\begin{cases} u_{thm} = Z_{ch} i_{chm} + u_{chm} \\ u_{phm} = i_{shm} Z_{sh} \\ u_{phm} / u_{thm} = n \\ i_{shm} / i_{chm} = -1/n \\ u_{cm} = u_{c1} + u_{chm} \le V_{dc} \\ V_{dcN} = V_{dc} / N \\ M = u_{cm} / V_{dc}, M \in (0,1] \\ M_1 = u_{c1} / V_{dc}, M_1 \in (1, M) \end{cases} \tag{1}$$

where the subscript m denotes the amplitude and h the h-harmonic order. V_{dc} is the total DC voltage of the CSH. $u_{c1}$is the fundamental of u_c.

Then we derive the amplitude of the harmonic current injected into the traction network as:

$$i_{shm} = \frac{(M - M_1) N V_{dcN}}{Z_{sh}/n + n Z_{ch}} \tag{2}$$

A large N can increase i_{shm} and decrease V_{dcN}, while the control strategy will be more complicated and it will be more difficult to balance the voltage of DC side. Although a small n leads to a large harmonic current, it needs more H-bridge modules to be cascaded due to high secondary-winding voltage of the transformer. Overly large L_c increases the damping of the control system, but the harmonic current may decrease. Therefore, the determination of the circuit parameters is a problematical issue due to the mutual influence among them. Based on the comprehensive consideration of constraint conditions between different factors in (2) and the experiment by trial and error, the parameters of this device are determined as listed in Table II.

B. Principle of operation

The device is designed as a harmonic generator to test the impedance of the traction network when there are no locomotives in the electric railway. The illustration of the impedance of the traction network is displayed in Fig. 4.

To facilitate the process of impedance measurement, the following steps are considered:

i. injection of h-order harmonic current into the traction network;

ii. samples of current signal, i_s, and voltage signal, u_p;

iii. application of DFT (Discrete Fourier Transformation) to the two signals respectively;

iv. calculation of h-order harmonic impedance by result of step iii, $i_s(h)$ and $u_p(h)$;

…… (repeat step ***i***~***iv*** until h=5000)

The implementation process of the test device is shown in Fig. 5. The impedance-frequency characteristic is acquired by a frequency scanning experiment.

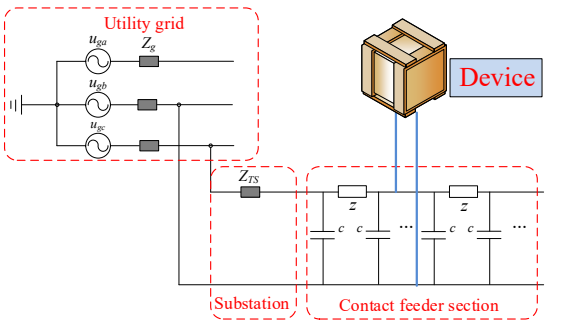

Fig. 4 Illustration showing the test of the impedance of traction network

TABLE II
Parameters of the Test Device

Symbols	Main circuit parameters	Values
S	Power capacity	150kVA
n	Transformation ratio of the transformer	20:1
N	Number of cascaded H-bridge	5
L_c	Inductance of the reactor	3mH
I_s	Rate current of the transformer	5.45A

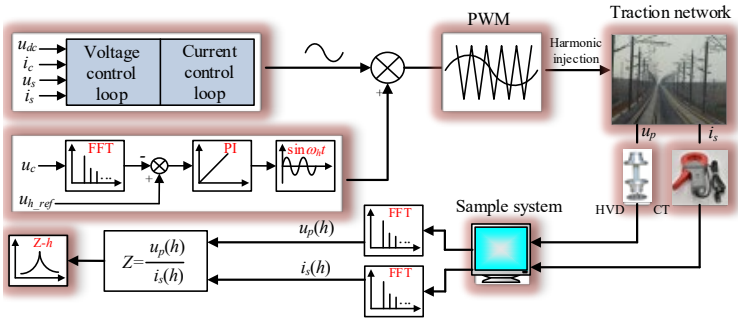

Fig. 5. Implementation process of the test device and impedance frequency responses calculation

The double closed-loop control algorithm, which is composed of the outer voltage control loop and the inner current control loop, outputs the sinusoidal modulation wave and maintains the DC side voltage stable to regulate the active power of the device. The schematic diagram of the double closed-loop control is shown in Fig. 6(a). The DC voltage outer loop controller (DVC) provides the amplitude reference value for the current inner loop controller (ACC). Then the sinusoidal current reference of the ACC is generated through the synchronization with the line voltage by the phase lock loop (PLL). The ACC outputs the modulation wave and maintains the current tracking its reference value.

Then, the harmonic injection is conducted by adding the harmonic voltage reference to the modulation wave of the CSH modules. As depicted in Fig. 5, u_{ch}, h-order harmonic voltage of CSH modules, is regulated to follow u_{h_ref}, the harmonic voltage reference. By pulse width modulation (PWM) of the CSH modules, harmonic voltage is produced in the CSH modules and then harmonic current appears in the traction network. The device works as a harmonic voltage source. So the harmonic current is determined by both the reference value of the harmonic voltage and the impedance of the traction network. Moreover, there is little content of the background harmonic because there is no locomotive in the railway line. When the device does not start, the harmonic

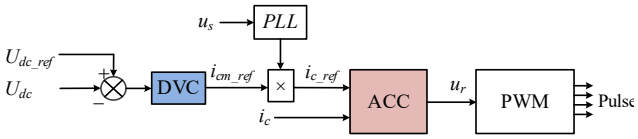

(a) The schematic diagram of the double closed-loop control

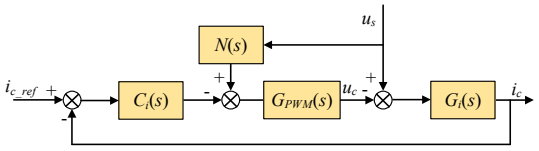

(b) The block diagram of the current control loop

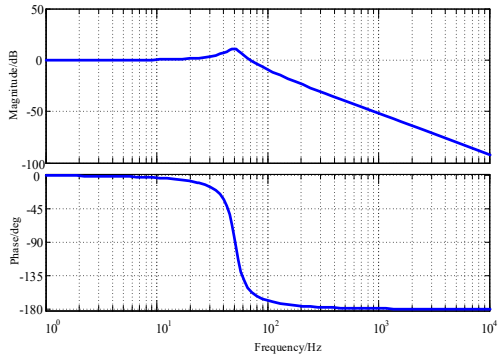

(c) The bode diagram of frequency response of the current controller

Fig. 6. Block diagram and bode diagram of current control loop displaying current attenuation at higher frequencies than 100Hz

content is lower than 0.1%. As a result, the harmonic voltage generated by this device is the dominated harmonic source.

This algorithm avoids adding a harmonic current reference to i_s directly because i_s cannot accurately follow the harmonic current reference at high frequencies for low bandwidth of the current control loop. The block diagram of the current control loop is illustrated in Fig 6(b). As shown in Fig. 6(b), G_i(s) is the transfer function of the controlled object, G_{PWM}(s) is the transfer function of the signal sample delay and the PWM process, C_i(s) is the current controller (using the proportional controller), and N(s) is the transfer function of the voltage feed-forward.

When the voltage feed-forward is not considered, the transfer function of the current control loop can be derived as:

$$H_{ci}(s)=\frac{C_i(s)G_{PWM}(s)G_i(s)}{1+C_i(s)G_{PWM}(s)G_i(s)} \tag{3}$$

The proportional controller is adopted in the inner current control loop due to the limited hardware resource. The bode diagram of the transfer function in (3) is displayed in Fig. 6(c). It indicates that the current attenuates heavily at high frequencies. Therefore, it is not effective to regulate the harmonic injection in the current control loop directly. It is necessary to adding the harmonic voltage reference to the modulation wave of the CSH modules through an independent harmonic control loop as shown in Fig 5. This strategy ensures that the current is neither too large nor too small. As a result, the harmonic injection method conducts the impedance measurement without impact on the normal operation of the traction network.

The phase-shifted carrier PWM is applied to the CSH. Compared with the single module which can output two levels or three levels, the multilevel cascaded H-bridge can achieve high equivalent switching frequency and high bandwidth. As a result, the device can inject harmonic current of higher frequency into the traction network. Therefore, the impedance measurement can be up to higher frequency.

The HVD transfers the voltage of traction network into a low voltage which can be sampled by the data acquisition system. Its 50Hz withstand voltage level is as high as 100kV and the voltage division ratio is 10000:1. At the frequency range from 10Hz ~1MHz, the measurement error is no more than 1%. The CT transfers the current of traction network into a low current. Its measurement error is 1% and the range of work frequency is 50Hz~100kHz. For the sample system, the sample rate is 50MHz/s and the storage depth is 128kb for every channel.

C. Power flow analysis

The test device injects a harmonic current into the traction network based on the layer control strategy. Its outstanding characteristic is that there is no external power supply apart from the traction power supply of the electrical railway. As a result, the device outputs harmonic power into the traction network when it keeps the DC voltage stable. The power flow is different from that of the average converter without harmonic generation control strategy. As shown in Fig. 3, the power source of the traction network is u_s, 27.5kV/50Hz. Then, the equivalent impedance of the traction network is converted to the secondary winding of the transformer as R_s' and L_s'. The leakage impedance of the transformer is included in R_c and L_c. The voltage and current of the power source are also converted to the secondary winding as u_s' and i_s' respectively. The source voltage can be expressed as:

$$u_s' = U_1 \sin(\omega_1 t)$$

The source current can be expressed as:

$$\begin{aligned} i_s' &= I_1 \sin(\omega_1 t+\alpha_1) + I_h \sin(h\omega_1 t+\alpha_h) + \\ &\sum_{n=2,n\neq h}^{\infty} I_n \sin(n\omega_1 t+\alpha_n), \quad h\geq 2 \end{aligned} \tag{4}$$

where the first item is the fundamental component, the second item is the specific harmonic current which is injected into the traction network from the test device, and the last item is the other harmonic current which exists in the main circuit due to the switching of the converters. The last item can be omitted due its small value. Then the instantaneous power which flows to the CSH can be derived as:

$$\begin{aligned} P_{csh} &= u_s' i_s' - i_s'^2(R_s'+R_c) - i_s'(L_s'+L_c)\frac{di_s'}{dt} \\ &= P_0 + \underbrace{P_2 + P_{h-1} + P_{h+1} + P_{2h}}_{\tilde{P}} \end{aligned} \tag{5}$$

where

$$P_0 = \frac{U_1 I_1}{2}\cos\alpha_1 - \frac{(R_s'+R_c)I_1^2}{2} - \frac{(R_s'+R_c)I_h^2}{2}$$

$$P_2 = -\frac{U_1 I_1}{2}\cos(2\omega_1 t+\alpha_1) + \frac{(R_s'+R_c)I_1^2}{2}\cos(2\omega_1 t+2\alpha_1)$$

$$-\frac{(L_s'+L_c)\omega_1 I_1^2}{2}\sin(2\omega_1 t+\alpha_1)$$

$$P_{h-1}=\frac{U_1 I_h}{2}\cos[(h-1)\omega_1 t+\alpha_h]-(R_s'+R_c)I_1 I_h\cos[(h-1)\omega_1 t]+\frac{(h-1)(L_s'+L_c)\omega_1 I_1 I_h}{2}\sin[(h-1)\omega_1 t+\alpha_h-\alpha_1)]$$

$$P_{h+1}=-\frac{U_1 I_h}{2}\cos[(h+1)\omega_1 t+\alpha_h]+(R_s'+R_c)I_1 I_h\cos[(h+1)\omega_1 t+2\alpha_1]-\frac{(h+1)(L_s'+L_c)\omega_1 I_1 I_h}{2}\sin[(h+1)\omega_1 t+\alpha_h+\alpha_1)]$$

$$P_{2h}=\frac{(R_s'+R_c)I_h^2}{2}\cos(2h\omega_1 t+2\alpha_h)-\frac{h(L_s'+L_c)\omega_1 I_h^2}{2}\sin(2h\omega_1 t+2\alpha_h)$$

In (5), there are five components: P_0 is the constant component, and P_2, P_{h-1}, P_{h+1}, P_{2h} are all the fluctuating components which flow between the traction network and the CSH. The fluctuating components relate to the fundamental current and harmonic current. For P_0, the first two items are the fundamental power and the positive sum means that CSH absorbs fundamental power from the traction network. In contrast, the negative last item means that CSH can transfer harmonic power to the traction network.

The power balance relationship between the DC side and the AC side of the CSH is:

$$P_0+\tilde{P}=\sum_{k=1}^{5}C_1\frac{du_{dck}}{dt}u_{dck}+\sum_{k=1}^{5}\frac{u_{dck}^2}{R_k} \tag{6}$$

The DC voltage of the module u_{dck} is divided into a steady-state DC voltage and a fluctuating voltage:

$$u_{dck}=U_{dc}+\tilde{u}_{dc} \tag{7}$$

Inserting (7) into (6), it can be derived:

$$\tilde{P}=\sum_{k=1}^{5}C_1\frac{d\tilde{u}_{dck}}{dt}U_{dc}+\sum_{k=1}^{5}\frac{2\tilde{u}_{dck}}{R_k}U_{dc} \tag{8}$$

According to the power relationship in (5) and (8), the device only absorbs power from the traction network and then it can generate harmonic power into the traction network. In addition, the DC voltage of the module is maintained stable by means of the appropriate control strategy. Therefore, there is no need for an extra power source, which makes it convenient for on-site measurement and reduces the cost of the device.

III. On-site Test in an Electric Railway

A. Location arrangement of on-site test

The impedance of the traction network is influenced by not only the railway itself but also the utility grid. Moreover, the traction network is a complex system compromising various conductors whose parameters vary with different installation circumstance, various conductor types, and complex network structures. Consequently, it is difficult to establish the platform of the actual traction network with a complete line of distributed parameters. As a result, the validation of this test device in an actual electric railway is necessary to obtain the impedance of the traction network. The on-site test is conducted in the front and the end of the power supply arm. There are no locomotives running on the line, otherwise the impedance will include the impedance of the locomotive. In addition, there is no need to shut off the electricity supply of the traction substation during the test procedure.

The device is installed in the traction network of a new-built line between Beijing and Shenyang, which is the auto-transformer (AT) feeding system. There are two parallel lines: one is from Beijing to Shenyang (called the downgoing line), the other is from Shenyang to Beijing (called the upgoing line).

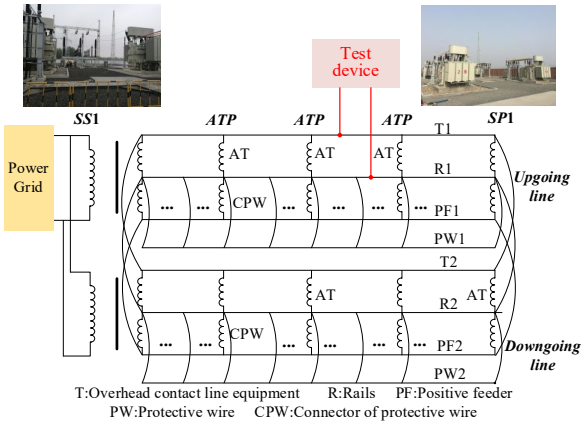

(a) Location of the test device in one feeding section of the new-built railway

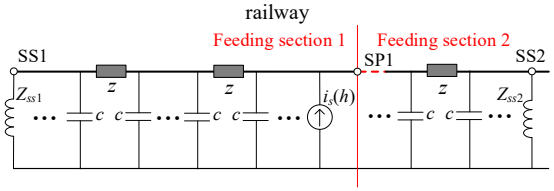

(b) Simplified equivalent circuit with distributed parameters

Fig. 7 Schematic diagram of on-site test arrangement in a new-built railway of Beijing-Shenyang

The installation location of the test device is displayed in Fig. 7(a). The test device is installed between the overhead contact line and the rails. The length of the experimental section is up to 24.65km between a traction substation and the adjacent section post. Substation (SS) transfers three-phase electricity of utility power grid into single-phase electricity which is needed for the upgoing and downgoing locomotives. There are two auto-transformers in the Auto-Transformer Post (ATP). The Section Post (SP) is set between two feeding sections. As a result, the traction network is divided into several sections powered by different SSs. When one of the SSs fails, SP can connect the two sections which can receive electricity from the same feeding section (this mode is called over-zone feeding). In Fig. 7(a), SS1 and SP1 are, respectively, the head and terminal of one feeding section.

This test aims at obtaining the impedance for different

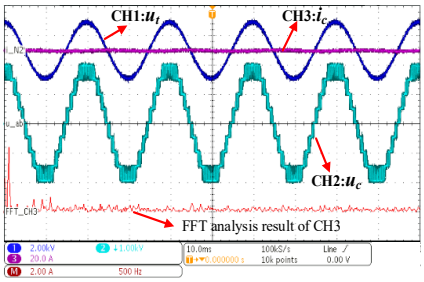

Fig. 8 Waveforms and harmonic spectrum for the converter side when the device does not inject harmonic current (CH1: voltage of converter side; CH2: voltage of CSH; CH3: current of converter side)

locations of the device in the traction network because the impedance characteristics vary at different sites. In order to illustrate the impedance which is going to be measured, this traction network is represented by a simplified equivalent circuit of overhead contact line and rails. As shown in Fig. 7(b), there are distributed parameters in this equivalent circuit: c is the parallel capacitance and z is the series impedance per unit length of the overhead contact line. Firstly, we place this device in SS1 and perform the experiment to acquire the impedance seen from the head. Secondly, by installing the device in SP1, we can measure the impedance seen from the terminal. In order to obtain the impedance of the middle position, we conduct a switching operation so that the SP1 becomes the middle position of the traction network between SS1 and SS2.

B. Harmonic injection performance of the device

The test device measures the impedance of the traction network by injecting harmonic currents into the railway. The performance of harmonic injection influences the accuracy of the impedance measurement. A harmonic current is generated by the CSH and then injected into the traction network. Therefore, the harmonic injection performance of the device is evaluated from two sides respectively: network side and converter side. As shown in Fig. 3, the network side is connected with the converter side by the step-down transformer.

In this device, the CSH with a harmonic control block plays an important role in generating the harmonic current. Figure 8 shows the performance of the CSH when the device does not inject the harmonic current into the traction network. As shown in the CH1 signal in Fig. 8, the voltage of converter side, u_t, is a pure sinusoid without any harmonics. For the CH3 signal, the current amplitude of converter side, i_c, is very small because there is no load (no locomotive) on the railway line. Moreover, there is low harmonic content in current waveform, which is generated by the pulse width modulation of the CSH. For the CH2 signal, the voltage of CSH is a typical PWM switching waveform without any distortion. During the on-site test, the oscilloscope is used to observe the real-time voltage and current waveforms of the CSH because the host compute plays an important role in monitoring the normal operation and combining the various parts of the whole system.

When the device injects the harmonic current into the traction network, the harmonic voltage response is produced. Figure 9 presents the waveforms and harmonic spectra for the converter side when harmonics at 800Hz, 1525Hz and 3250Hz are set in the control strategy to inject into the traction network. As shown in Fig. 9(a), (b), (c), a high value of harmonic current is generated by the CSH so that the current waveform distortion occurs. When the harmonic reference at a certain frequency is given to the control strategy, only the harmonic current at this frequency is dominant and the harmonic currents at the other frequencies are very small.

Accordingly, the harmonic response is produced in u_t, the voltage of converter side. The PWM voltage of CSH in Fig. 9 presents obvious distortion. In Fig. 9(a), harmonic current amplitude at 800Hz is as high as 10A. That is to say, this

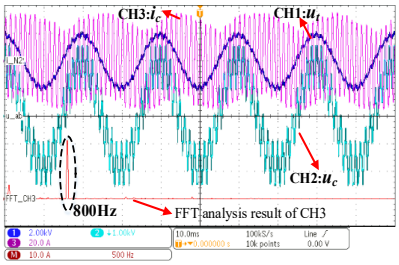

(a) Waveforms and harmonic spectrum when 800Hz harmonic current is injected

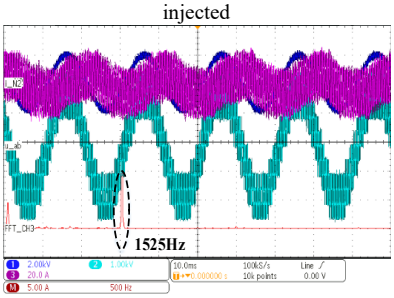

(b) Waveforms and harmonic spectrum when 1525Hz harmonic current is injected

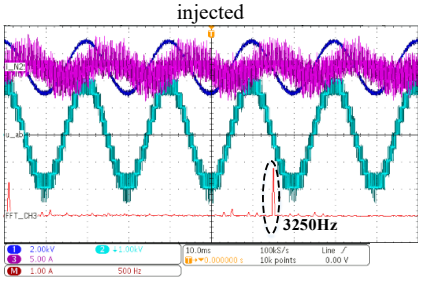

(c) Waveforms and harmonic spectrum when 3250Hz harmonic current is injected

Fig. 9 Waveforms and harmonic spectra for the converter side when the device injects different harmonic currents into the traction network

device has a good ability to generate a sufficient harmonic current which is beneficial for improving the accuracy of the impedance measurement to some extent. The high harmonic current will not affect the traction network performance because there is no locomotive on the railway during the on-site test. As shown in Fig. 9(b), this device can generate a sub-harmonic current. If there are locomotives running, background harmonics should be taken into consideration. The sub-harmonic current is a solution to eliminate the influence of background harmonics. In Fig. 9(c), this device can generate a harmonic current at high frequency. This shows that the device can measure the impedance at a wider frequency range.

The harmonic current generated by the CSH flows into the traction network via the step-down transformer. The waveforms and harmonic spectra for the network side are presented in Fig. 10 when the harmonic current at 550Hz is produced. As shown in Fig. 10(a) and (b), the current of traction network contains a noticeable harmonic component at 550Hz, which features the highest value among all harmonics. The current is not a pure sinusoidal waveform due to the harmonic injection. The amplitude of harmonic current at 550Hz is 2.6 times higher than the fundamental current. In Fig. 10(c) and (d), the amplitude of the harmonic voltage response at 550Hz is the highest among all the harmonic voltages. Then, the impedance can be calculated by the

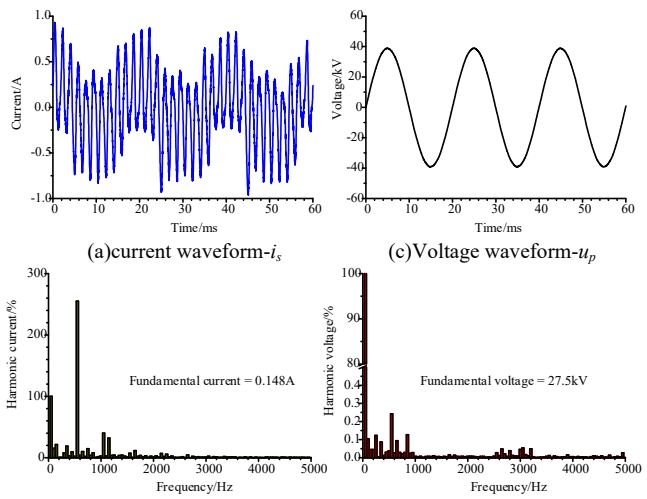

(a)current waveform-i_s (c)Voltage waveform-u_p

(b)harmonic spectrum of current (d)harmonic spectrum of voltage

Fig. 10 Waveforms and harmonic spectra of voltage and current in traction network

harmonic current injection and harmonic voltage response in the traction network.

C. *Measurement results of frequency-dependent impedance*

The impedance of the traction network can be calculated in the integrated software of the host computer by a frequency sweeping experiment. The on-site test is conducted in two positions within the network, SS1 and SP1 respectively, as shown in Fig. 7 (b). Normally, this experimental line adopts the AT feeding mode. As a result, SS1 is the head of the line and SP1 is the terminal. However, when the traction network adopts the over-zone feeding, SS1 is the head as usual, but SP1 is the middle of a longer line between two substations. The over-zone feeding makes the feeding section longer.

Figure 11 shows the impedance-frequency plots obtained in SS1 and SP1 respectively. For all plots, the peak value is the typical feature, which is different from the RL (resistance and inductance) parameter of the simple equivalent circuit for the traction network.

The impedance relates to the length of the traction network and the location of the test device. That is to say, when the train runs in different locations of different railway lines, the impedance of traction network displays different characteristics seen from the train side. Different from the impedance of the utility grid, the impedance of the traction network cannot be regarded as a constant parameter.

The maximum of the magnitude of the impedance indicate that there is a risk of harmonic resonance. As a result, this device can be applied to identify the frequency of the harmonic resonance through the magnitude-frequency plots.

Comparing curves (a1) with (b1) in Fig. 11(a), although the maximum of impedance magnitude seen from the head position is higher than that of the terminal position, both the impedance results present maximum magnitude at the same frequency, nearly 1350Hz. As shown in curves (a2) and (b2), the phase changes from approximately 90 to -90 at the maximum magnitude. Namely, the impedance is almost purely inductive at low frequency, and it turns to almost purely capacitive at this frequency. This frequency is called as the *phase-crossing frequency*. It indicates that there is a risk of occurrence of the harmonic resonance. Obviously, there is also another phase-crossing frequency but the extreme magnitude is too low. This kind of phase-crossing frequency will not give

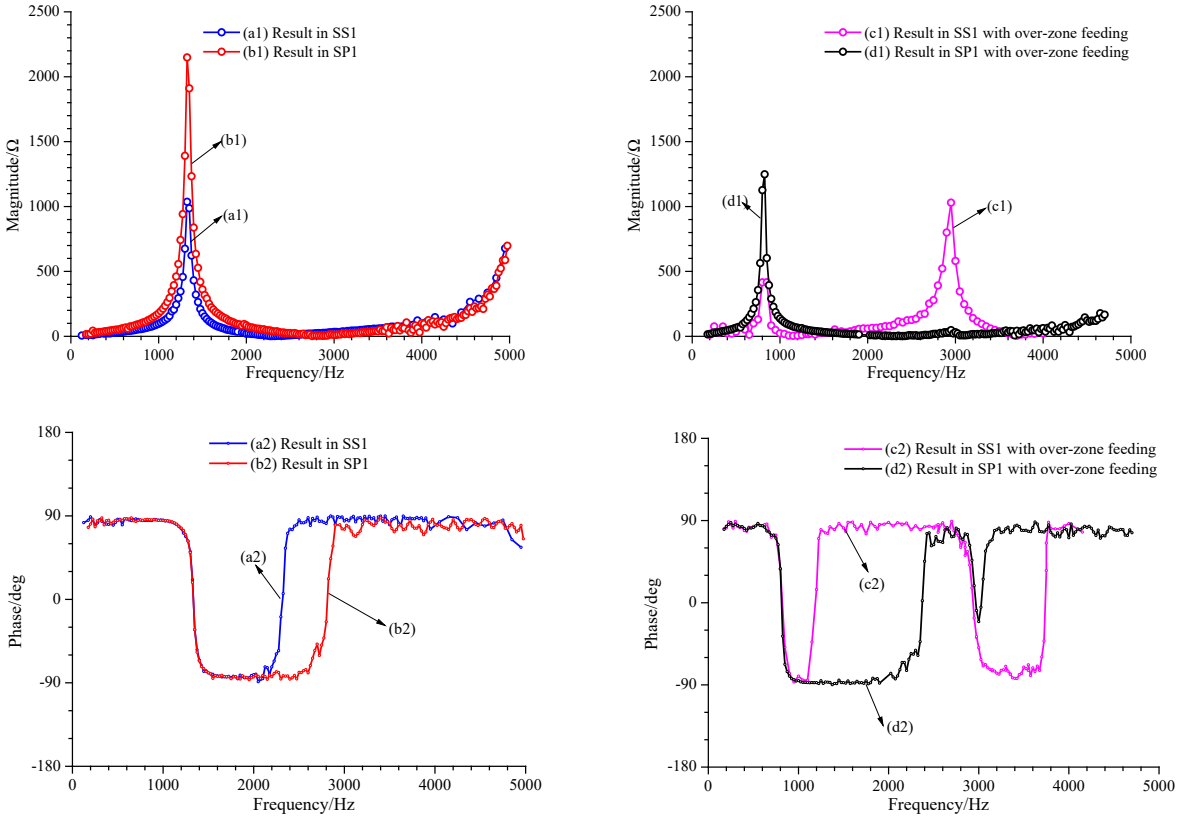

(a)Result when the power supply system is normal (b) Result when the over-zone feeding supply is adopted

Fig. 11 Impedance-frequency plots obtained in a new-built railway

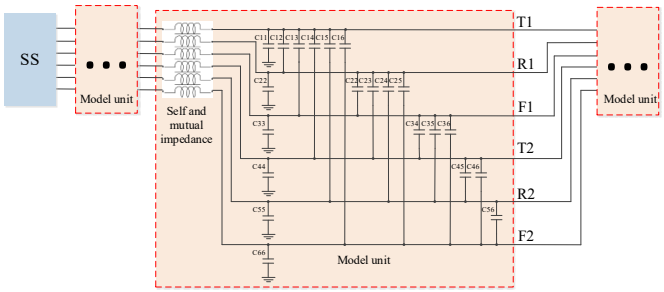

Fig. 12 Simulation model of the traction network

rise to harmonic resonance. Furthermore, it should be note that there is trajectory derivation for the phase at higher frequency due to the influence of the decreasing phase-angle precision of the current sensor and the higher electromagnetic noise introduced from the environment.

When the feeding section adopts over-zone feeding, as shown in curve (c1), the magnitude-frequency plot obtained in SS1 (head of the traction network) shows that there are two extreme points at different frequencies, 850Hz and 3000Hz. On the contrary, for curve (d1), there is only one maximum magnitude. But comparing curves (c1) with (d1), both extreme values appear at the same frequency, 850Hz. Moreover, there are phase crossing points at 850Hz in Fig. 11(b). As shown in the curve (b1) of Fig. 11(a) and curve (d1) of Fig. 11(b), the first extreme point of the magnitude appears at a lower frequency when the traction network is longer.

Therefore, the impedance of traction network cannot simply be regarded as an RL parameter due to the distribution parameter characteristic. The impedance plots exhibit the unique characteristics of the network system. On one hand, it corresponds with the characteristic of the high-order harmonic resonance in electric railway. For one electric railway, the frequencies of the harmonic resonance accidents occurring at different time are the same according to the theoretical analysis and the field test data [28, 29]. On the other hand, the simulation result also validates the on-site test of this device [30].

The identification of the maximum of the magnitude-frequency plot is important for the harmonic resonance of the electric railway because it means that a small harmonic injection at the frequency of the maximum magnitude can provoke high harmonic responses in the traction network. Based on these measurement results, it can be seen that the length of the traction network has an impact on the frequency of maximum impedance. However, the position of harmonic injection only influences the magnitude of the impedance and has no impact on the frequency of maximum impedance.

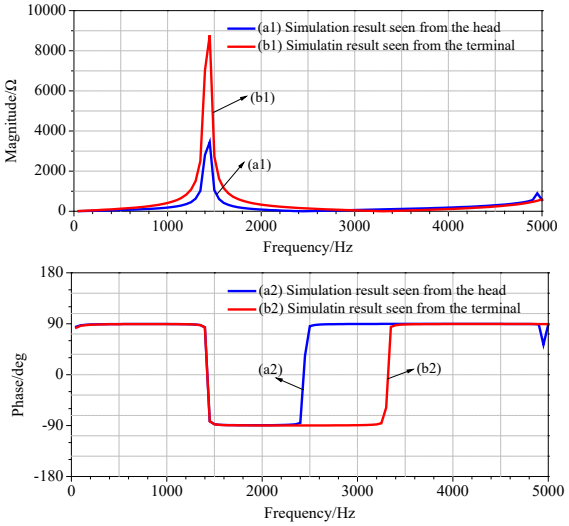

Fig. 13 Simulation result of frequency-dependent impedance for the 30km traction network

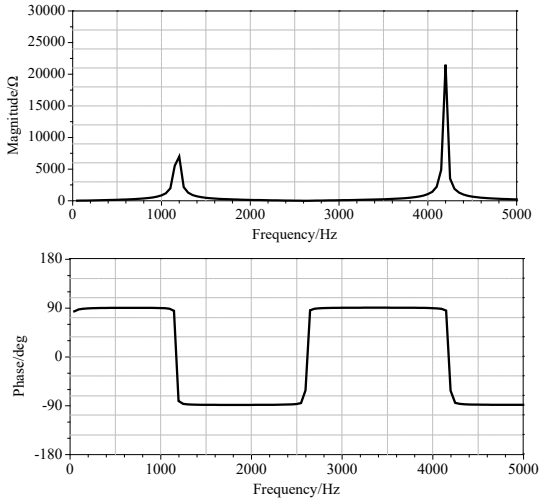

Fig. 14 Simulation result of frequency-dependent impedance for the 40km traction network

D. Comparison with the simulation result

Time-domain simulation is a popular and convenient method to simulate the various characteristics of the real systems. It is an important issue to verify the effectiveness of the simulation model through conducting experiment in the real systems. With respect to the simulation model of the impedance of the traction network, it is still challenging to validate its effectiveness because it is not so practicable to establish the down-scale prototype in the laboratory.

The traction network is a complex system with several conductors. It is difficult to establish a detailed model which includes all the conductors. Based on the simplified calculation of the network elements and the truncation treatment of feeding system in [9], the entire traction network is modeled as an equivalent 6-conductor line consisting of uplink and downlink contact lines (T1, T2), rails (R1, R2) and feeders (F1, F2). The entire feeding section can be cut into several units by the shunt or series elements. As shown in Fig. 12, the simulation model is established in Matlab/Simulink software. The self and mutual impedance parameters of the conductors are calculated by Carson-Pollaczek equations. The capacitance between the conductors and ground are added in the simulation model. In addition, the SS is modeled as a voltage source with a series RL (resistance-inductance) circuit.

The simulation result is shown in Fig. 13 when the length of the traction network is 30km. The curves (a1), (a2) and (b1), (b2) are the impedance-frequency characteristic seen from the head and the terminal of the traction network respectively. Both the maximums are located at 1450Hz but the values differ. The maximum magnitude of the impedance seen from the terminal is higher than the one seen from the head. And the impedance changes from almost purely inductive to capacitive as shown in curves (a2) and (b2). This trend matches the on-site test result of Fig. 11.

When the length of the traction network increases to 40km, the simulation result is displayed in Fig. 14. There are two extreme points in the magnitude-frequency plots. The first one is located at 1150Hz, which is lower than the frequency of maximum magnitude in Fig. 13. These simulation results

indicate that the frequency of maximum decreases when the feeding section of the railway becomes longer. Moreover, the location of the harmonic injection only affects the value of the maximum magnitude but not the frequency, similar to the experimental results.

From these results it can be seen that there is a good consistency between the simulated and tested results for the influence of the length and harmonic injection on the frequency-dependent impedance. Compared to the simulation of the multi-conductor model, the designed test device is shown to be an effective instrument to obtain the impedance-frequency plots without the need for knowing the structure and the parameter of the traction network. Furthermore, the consistence between the simulation and test indicates that the multi-conductor model can be used to obtain the impedance of the traction network in case that the parameters of the simulation model are proper.

IV. Conclusions

This paper presents an industrial device to measure frequency-domain impedance of the traction network based on the injection of harmonic currents. On the one hand, the traction network is still powered during the measurement so that the influence of the utility grid is taken into consideration. On the other hand, there is no need for an extra power source because this device can draw power from the traction network to maintain the DC-link voltage stable and, at the same time, generate harmonics. Moreover, this device can measure the impedance of the traction network of various supply modes and complicated parameters, regarding the traction network as a black box. Moreover, this device does not disturb the normal operation of the locomotives because the interval between harmonic injections can be controlled by the host computer.

By adding harmonic voltage reference into the modulation wave of CSH modules, harmonic currents of different frequencies are produced in the traction network. Following this, due to difficulties in setting up the prototype of the traction network in the laboratory, the on-site test is conducted in a new line of Beijing-Shenyang. The obtained impedance-frequency plots indicate that there is a maximum magnitude for every traction network at a different frequency. The value of the maximum magnitude relates to the length of the traction network and the location of the harmonic injection. The on-site test results in the actual railway can be applied to determine the resonance frequency before a new-built line is put into use so that the harmonic resonance can be avoided by taking effective measures in advance. In addition, the impedance of the traction network can be applied to carry out the small-signal stability analysis of the electric railway and the assessment of the mitigation methods of the harmonic resonance.

References:

[1] H. Cui, W. Song, H. Fang, X. Ge, and X. Feng, "Resonant harmonic elimination pulse width modulation-based high-frequency resonance suppression of high-speed railways," *IET Power Electronics,* vol. 8, pp. 735-742, 2015.

[2] H. Tao, H. Hu, X. Zhu, Y. Zhou, and Z. He, "Harmonic Instability Analysis and Suppression Method Based on αβ-Frame Impedance for Trains and Network Interaction System," *IEEE Transactions on Energy Conversion,* vol. 34, pp. 1124-1134, 2019.

[3] S. Luis, M. Lluis, J. M. Juan, P. Joaquin, and M. Cheah-Mané, "Electrical Resonance Instability Study in Traction Systems,", 2016, pp. 133-138.

[4] W. Song, S. Jiao, Y. W. Li, J. Wang, and J. Huang, "High-Frequency Harmonic Resonance Suppression in High-Speed Railway Through Single-Phase Traction Converter With LCL Filter," *IEEE Transactions on Transportation Electrification,* vol. 2, pp. 347-356, 2016.

[5] S. Hu, Z. Zhang, Y. Chen, G. Zhou, Y. Li, L. Luo, Y. Cao, B. Xie, X. Chen, B. Wu, and C. Rehtanz, "A New Integrated Hybrid Power Quality Control System for Electrical Railway," *IEEE Transactions on Industrial Electronics,* vol. 62, pp. 6222-6232, 2015.

[6] P. C. Tan, P. C. Loh and D. G. Holmes, "A Robust Multilevel Hybrid Compensation System for 25-kV Electrified Railway Applications," *IEEE Transactions on Power Electronics,* vol. 19, pp. 1043-1052, 2004.

[7] J. Holtz and H. J. Kelin, "The propagation of harmonic currents generated by inverter-fed locomotives in the distributed overhead supply system," *IEEE Transactions on Power Electronics,* vol. 2, pp. 168-174, 1989.

[8] P. C. Tan, P. C. Loh and D. G. Holmes, "Optimal Impedance Termination of 25-kV Electrified Railway Systems for Improved Power Quality," *IEEE Transactions on Power Delivery,* vol. 20, pp. 1703-1710, 2005.

[9] W. Mingli, C. Roberts and S. Hillmansen, "Modelling of AC feeding systems of electric railways based on a uniform multi-conductor chain circuit topology," in *IET Conference on Railway Traction Systems (RTS 2010)*, Stevenage, 2010, p. 1-5.

[10] H. Lee, C. Lee, G. Jang, and S. Kwon, "Harmonic Analysis of the Korean High-Speed Railway Using the Eight-Port Representation Model," *IEEE Transactions on Power Delivery,* vol. 21, pp. 979-986, 2006.

[11] L. Battistelli, M. Pagano and D. Proto, "2×25-kV 50 Hz High-Speed Traction Power System: Short-Circuit Modeling," *IEEE Transactions on Power Delivery,* vol. 26, pp. 1459-1466, 2011.

[12] A. Mariscotti and P. Pozzobon, "Resistance and Internal Inductance of Traction Rails at Power Frequency: A Survey," *IEEE Transactions on Vehicular Technology,* vol. 53, pp. 1069-1075, 2004.

[13] G. Lucca, "Per unit length parameters of a multiconductor line with earth return inside a tunnel," *IEEE Transactions on Electromagnetic Compatibility,* vol. 42, pp. 6-15, 2000.

[14] A. Dolara, M. Gualdoni and S. Leva, "Impact of High-Voltage Primary Supply Lines in the 2 × 25 kV–50 Hz Railway System on the Equivalent Impedance at Pantograph Terminals," *IEEE Transactions on Power Delivery,* vol. 27, pp. 164-175, 2012.

[15] A. S. Morched and P. Kundur, "Identification and modelling of load characteristics at high frequencies," *IEEE Transactions on Power Systems,* vol. 2, pp. 153-159, 1987.

[16] W. Wang, E. E. Nino and W. Xu, "Harmonic impedance measurement using a thyristor-controlled short circuit," *IET Generation, Transmission & Distribution,* vol. 1, pp. 707-713, 2007.

[17] W. Xu, E. E. Ahmed, X. Zhang, and X. Liu, "Measurement of network harmonic impedances: practical implementation issues and their solutions," *IEEE Transactions on Power Delivery,* vol. 17, pp. 210-216, 2002.

[18] S. T. Mak, "A New Method of Generating TWACS®Type Outbound Signals for Communication on Power Distribution Networks," *IEEE Transactions on Power Apparatus and Systems,* vol. PAS-103, pp. 2134-2140, 1984.

[19] M. Sumner, B. Palethorpe, D. W. P. Thomas, P. Zanchetta, and M. C. Di Piazza, "A technique for power supply harmonic impedance estimation using a controlled voltage disturbance," *IEEE Transactions on Power Electronics,* vol. 17, pp. 207-215, 2002.
[20] T. Roinila, M. Vilkko and J. Sun, "Online Grid Impedance Measurement Using Discrete-Interval Binary Sequence Injection," *IEEE Journal of Emerging and Selected Topics in Power Electronics,* vol. 2, pp. 985-993, 2014.
[21] L. Asiminoaei, R. Teodorescu, F. Blaabjerg, and U. Borup, "Implementation and Test of an Online Embedded Grid Impedance Estimation Technique for PV Inverters," *IEEE Transactions on Industrial Electronics,* vol. 52, pp. 1136-1144, 2005.
[22] M. Cespedes and J. Sun, "Adaptive Control of Grid-Connected Inverters Based on Online Grid Impedance Measurements," *IEEE Transactions on Sustainable Energy,* vol. 5, pp. 516-523, 2014.
[23] H. W. M. Smulders and H. A. Prins, "Fast and efficient determination of Eigenfrequencies of railway systems," in *2015 IEEE International Instrumentation and Measurement Technology Conference (I2MTC) Proceedings* Pisa, Italy, 2015.
[24] M. Jaksic, Z. Shen, I. Cvetkovic, D. Boroyevich, R. Burgos, C. DiMarino, and F. Chen, "Medium-Voltage Impedance Measurement Unit for Assessing the System Stability of Electric Ships," *IEEE Transactions on Energy Conversion,* vol. 32, pp. 829-841, 2017.
[25] Z. Liu, I. Cvetkovic, Z. Shen, D. Boroyevich, R. Burgos, and J. Liu, "Imbalance Mechanism and Balancing Control of DC Voltages in a Transformerless Series Injector Based on Paralleled H-Bridge Converters for AC Impedance Measurement," *IEEE Transactions on Power Electronics,* vol. 34, pp. 8175-8189, 2019.
[26] M. Petkovic, N. Hildebrandt, F. D. Freijedo, and D. Dujic, "Cascaded H-Bridge Multilevel Converter for a High-Power Medium-Voltage Impedance-Admittance Measurement Unit,", 2018, pp. 1-8.
[27] L. Wu and W. Mingli, "Single-phase cascaded H-bridge multi-level active power filter based on direct current control in AC electric railway application," *IET Power Electronics,* vol. 10, pp. 637-645, 2017.
[28] R. E. Morrison and M. J. Barlow, "Continuous Overvoltages on A.C. Traction Systems," *IEEE Transactions on Power Apparatus and Systems,* vol. PAS-102, 1983.
[29] K. Song, M. Wu, S. Yang, Q. Liu, V. G. Agelidis, and G. Konstantinou, "High-Order Harmonic Resonances in Traction Power Supplies: A Review Based on Railway Operational Data, Measurements and Experience," *IEEE Transactions on Power Electronics,* p. 1-1.
[30] R. Zhang, S. Liu, F. Lin, H. Cao, Y. Liu, and K. Han, "Resonance influence factors analysis of high-speed railway traction power supply system based on RT - LAB," in *2017 IEEE Transportation Electrification Conference and Expo*, Harbi,China, 2017, pp. 1-6.

Mingli Wu (M'09) was born in Hebei Province, China. He received his B.Sc. and M.Sc. degrees in Electrical Engineering from Southwest Jiaotong University, Chengdu, China, in 1993 and 1996, respectively, and his Ph.D. in Electrical Engineering from Beijing Jiaotong University, Beijing, China, in 2006.

Since 2008, he has been a Professor at the School of Electrical Engineering, Beijing Jiaotong University. His research areas include power supply for electric railways, digital simulation of power systems, and electric power quality.

Jing Li (S'18) received her B.Sc degree in Electrical Engineering from North China University of Water Resources and Electric Power, Zhengzhou, China, in 2013, and M. Sc degree from Beijing Jiaotong University, Beijing, China, in 2016. She is currently working toward her Ph.D. degree in Electrical Engineering at Beijing Jiaotong University. She was a Visiting Student at the Norwegian University of Science and Technology (NTNU), Trondheim, Norway, from October 2018 to 2019. Her research interests include power quality of electric railways and power electronics in power supply systems.

Qiujiang Liu (S'18) was born in Hebei province, China. He received his B.Sc., M.Sc. and Ph.D. degrees in Electrical Engineering from Beijing Jiaotong University, Beijing, China, in 2012, 2014 and 2018 respectively, where he is currently a Postdoctoral Researcher. His research interests include power quality of electric railways and power electronics in traction power supply systems.

Shaobing Yang (M'15) received the B.S. degree in electrical engineering from Shanghai Jiao Tong University, Shanghai, China, in 1995, and the M.S. and Ph.D degrees in electrical engineering from Beijing Jiaotong University, Beijing, China, in 2009 and 2016, respectively. He is an Associate Professor with the School of Electrical Engineering, Beijing Jiaotong University. His current research interests include power system simulation, load modeling, demand side management, electric power quality, and load forecasting for electric vehicles.

Marta Molinas (M'94) received the Diploma degree in electromechanical engineering from the National University of Asuncion, Asuncion, Paraguay, in 1992, the Master's of Engineering degree in information engineering from Ryukyu University, Nishihara, Japan, in 1997, and the Doctor of Engineering degree in electrical engineering from the Tokyo Institute of Technology, Tokyo, Japan, in 2000. She was a Guest Researcher with the University of Padova, Italy in 1998. From 2004 to 2007, she was a Postdoctoral Researcher with the Norwegian University of Science and Technology (NTNU), Trondheim, Norway, where she has been a Professor with the Department of Electric Power Engineering, from 2008 to 2014. She is currently a Professor with the Department of Engineering Cybernetics, NTNU. Her research interests include stability of complex power electronics systems, harmonics, oscillatory phenomena, and nonstationary signals from the human and the machine.

Dr. Molinas serves as an Editor for the IEEE JOURNAL OF EMERGING AND SELECTED TOPICS IN POWER ELECTRONICS and the IEEE TRANSACTIONS ON ENERGY CONVERSION. She is an Associate Editor of the IEEE TRANSACTIONS ON POWER ELECTRONICS and the IEEE TRANSACTIONS ON INDUSTRIAL ELECTRONICS.